Comprehensive Validation of Temperature and Humidity Profile Retrievals from FengYun-3E

Shuanghui Liu, Jian Xu, *Senior Member, IEEE*, Lin Chen, Hui Liu, Wenyu Wang, *Member, IEEE*, Jieying He, Songyan Zhu, *Member, IEEE*, Jiancheng Shi, *Fellow, IEEE*

***Abstract*—The FengYun (FY) meteorological satellites, equipped with combined microwave and infrared sensors, provide temperature and humidity profiles under both clear and cloudy conditions, supporting global atmospheric monitoring and weather forecasting. This study evaluates the FY-3E Vertical Atmospheric Sounding System (VASS) using collocated radiosonde observations, reanalysis data, and satellite measurements including the Cross-track Infrared and Microwave Sounder Suite (CrIMSS) onboard JPSS-1. Under all-sky conditions, VASS temperature profiles exhibit a correlation of 0.99 with radiosonde data, and humidity profiles reach 0.80. The temperature biases (RMSEs) are 0.63 K (3.07 K) under clear-sky, 0.82 K (3.56 K) under cloudy-sky, and 0.67 K (3.26 K) under all-sky conditions. The corresponding humidity biases (RMSEs) are 4.63% (18.36%), 6.21% (21.38%), and 4.76% (19.36%). As compared with CrIMSS products using coincident radiosonde data, the VASS retrievals show larger errors in both temperature and humidity, yet provide consistent and reliable atmospheric profiles under diverse conditions. These results confirm the current utility of FY-3E VASS in operational weather and climate services, while highlighting the need for continued algorithm development to further reduce retrieval uncertainties.**

***Index Terms*—FengYun-3E, VASS, temperature, humidity**

I. Introduction

UNDERSTANDING atmospheric temperature and humidity is essential for accurate weather forecasting and climate research. These observations are fundamental to studying atmospheric processes such as heat transfer, cloud formation, and precipitation. Temperature variations across different atmospheric layers affect stability and convection, whereas humidity distribution is critical for cloud development and the hydrological cycle. Analyzing these parameters helps predict severe weather events, track climate trends, and understand atmospheric dynamics on both regional and global scales.

This work was supported by the National Key Research and Development Program of China under Grant 2024YFB3907900. *(Corresponding author: Jian Xu.)*

Shuanghui Liu is with the Key Laboratory of Microwave Remote Sensing, National Space Science Center, Chinese Academy of Sciences, Beijing 100190, China, and also with the School of Electronic, Electrical and Communication Engineering, University of Chinese Academy of Sciences, Beijing 101408, China (email: liushuanghui@nssc.ac.cn).

Jian Xu, Wenyu Wang, Jieying He, and Jiancheng Shi are with the Key Laboratory of Microwave Remote Sensing, National Space Science Center, Chinese Academy of Sciences, Beijing 100190, China (xujian@nssc.ac.cn; wangwenyu@mirslab.cn; hejieying@mirslab.cn; shijiancheng@nssc.ac.cn).

Lin Chen and Hui Liu are with the National Satellite Meteorological Center (NSMC), China Meteorological Administration, Beijing 100081, China (email: chenlin@cma.gov.cn; liuhui@cma.gov.cn).

Songyan Zhu is with the School of Geography and Environmental Science, University of Southampton, Southampton SO17 1BJ, U.K. (email: Songyan.Zhu@soton.ac.uk).

Satellite remote sensing enables retrieval of atmospheric temperature and humidity profiles over broad areas where ground-based observations are sparse. In particular, spaceborne microwave and hyperspectral infrared (IR) sounders have greatly improved numerical weather prediction capabilities. Microwave measurements can penetrate clouds but are limited by their coarse spectral resolution [1]. In contrast, infrared sounders offer higher vertical resolution due to fine spectral sampling, although their sensitivity to clouds can significantly degrade retrieval accuracy [2], [3]. Temperature profiles from microwave sounders such as the Advanced Microwave Sounding Unit A (AMSU-A) [4], [5], the Advanced Technology Microwave Sounder (ATMS) [6], and the Microwave Limb Sounder (MLS) [7] are retrieved primarily using the O_2 absorption band. In contrast, infrared sounders including the Atmospheric Infrared Sounder (AIRS) [8], the Infrared Atmospheric Sounding Instrument (IASI) [9], and the Cross-track Infrared Sounder (CrIS) [10] derive temperature profiles from CO_2 absorption features. Humidity profiles are retrieved from water vapor absorption channels by sounders such as the Humidity Sounder for Brazil (HSB) [11], Microwave Humidity Sounder (MHS) [12], and ATMS [13]. These instruments collectively enable vertical sounding of the atmosphere through absorption features of key gases, forming the basis for global operational weather and climate products.

Recently, several satellite products for temperature and humidity have been retrieved through a combination of microwave and hyperspectral infrared observations. The National Oceanic and Atmospheric Administration (NOAA) retrieved vertical temperature profiles using the ATMS and the CrIS onboard the Suomi National Polar-orbiting Partnership (Suomi-NPP) satellite, utilizing the NOAA Unique Combined Atmospheric Processing System (NUCAPS) algorithm [14]. The Community Long-term Infrared Microwave Combined Atmospheric Product System (CLIMCAPS), developed with NASA support, obtains atmospheric temperature, water vapor, surface emissivity, reflectivity, and skin temperature by combining co-located infrared and microwave measurements from instruments onboard Aqua (AIRS and AMSU) and Suomi-NPP/JPSS (CrIS and ATMS) [15]. NUCAPS is developed for real-time operational applications, whereas CLIMCAPS is optimized primarily for long-term climate studies and scientific analysis. Similar to NUCAPS and CLIMCAPS, the FY-3E Vertical Atmospheric Sounding System (VASS) retrieves temperature and humidity profiles by combining measurements from the Hyperspectral Infrared Atmospheric Sounder (HIRAS-II), the Microwave Humidity Sounder (MWHS-II),

and the Microwave Temperature Sounder (MWTS-III) [16], and has been applied in both operational weather forecasting and long-term environmental monitoring.

Since the 1970s, China has independently developed the FengYun meteorological satellite system, which includes both polar orbit and geostationary satellites. FengYun-3E (FY-3E) is the world's first civilian meteorological satellite flying in an early morning orbit (approximately 5:30 AM local time). Launched in July 2021, FY-3E operates in a near-polar, sun-synchronous orbit at an altitude of 836 km, with a planned mission lifetime of eight years [17]. FY-3E satellite aims to provide global observations for numerical weather prediction assimilation, thereby enhancing the accuracy of weather forecasts. Additionally, it monitors various meteorological, oceanographic, and solar-terrestrial physics environments [17]. The HIRAS-II, MWHS-II, and MWTS-III instruments are onboard the FY-3E satellite. Collectively, these three instruments comprise the Vertical Atmospheric Sounding System (VASS). The temperature and humidity products generated by the FY-3E VASS were released on April 19, 2023. This study aims to assess the retrieval accuracy of FY-3E VASS temperature and humidity products under various atmospheric conditions and to support their potential use in international meteorological research and applications.

This paper is organized as follows: Section II introduces the satellite products (FY-3E VASS, JPSS-1 CrIMSS, and FY-4B GIIRS) and the radiosonde observations used in this study. Section III describes the validation methodology, including data preprocessing, statistical metrics, and spatiotemporal collocation criteria. Section IV evaluates the accuracy of FY-3E VASS retrievals using radiosonde observations as the reference, and compares their performance with CrIMSS, GIIRS, and ECMWF Reanalysis v5 (ERA5) across different regions and temporal scales. A summary and discussion are presented in Sect. V.

II. Overview of Datasets

In this study, we utilize three satellite-based sounding products and one radiosonde dataset. The satellite products include temperature and humidity profiles from FY-3E VASS, JPSS-1 CrIMSS, and FY-4B GIIRS. Radiosonde data are obtained from the Integrated Global Radiosonde Archive version 2 (IGRA2). Details of all datasets are described below.

A. FY-3E VASS products

The FY-3E VASS dataset provides global temperature and humidity profiles under both clear and cloudy sky conditions by combining infrared and microwave measurements. The operational retrieval algorithm employs a fast piecewise-defined neural network (PDNN), which integrates a measurement-dependent classification scheme with a principal component-based feedforward neural network [16]. The neural network consists of one input layer, three hidden layers (with 100, 50, and 30 neurons, respectively), and one output layer. The input vectors include the cosine of the HIRAS-II viewing zenith angle; brightness temperatures (BTs) from all channels of MWHS-II and MWTS-III, and BTs from 450 selected channels of HIRAS-II. The training targets are obtained from the ERA5 reanalysis data. An early stopping approach is used to prevent overfitting.

To improve retrieval accuracy under varying atmospheric conditions, the radiance data and training targets are classified into four broad categories: clear sky, light cloudiness, medium cloudiness, and heavy cloudiness, based on the differences between the observed and simulated BTs. These four categories are then jointly subdivided into 20 classes according to the BT of HIRAS surface channel 510, the BT of the MWHS water absorption channel 15, and surface elevation. Among these, Classes 18 and 19 are distinguished solely by surface elevation. Specifically, for heavy cloudiness conditions, if the BT of the HIRAS channel 510 is $\leq$ 255 K and surface elevation is $>$ 2 km, the profile is assigned to Class 18; otherwise, it is assigned to Class 19. Each class has its own dedicated neural network coefficients trained from the corresponding data subset. A rain cloud flag is also provided, based on the scattering differences between the BTs from the 50 GHz and 118 GHz temperature-sounding channels. For more details, please refer to Bai et al. [16].

The quality flag (QFlag) information for VASS temperature and humidity profiles is obtained from the corresponding netCDF files. A QFlag value of 1 indicates "good" retrievals; values of 2 or 3 represent "not bad" retrievals; and a value of 4 denotes "not good" retrievals. QFlags of 0 or any value greater than 4 represent "bad" retrievals and are excluded from the analysis. Additionally, QFlag values of 1 and 2 correspond to clear-sky conditions, whereas values of 3 and 4 indicate cloudy-sky conditions.

The QFlags are provided at each pressure level for both temperature and humidity profiles. The distribution of QFlag values used in this study is illustrated in Fig. 1. The proportion of valid retrievals (i.e., QFlag $= 1, 2, 3, 4$) increases with altitude, as the degraded accuracy in the lower atmosphere leads to the exclusion of more data due to stricter quality control. For temperature profiles, the percentages of retrievals with QFlag values of 1, 2, 3, and 4 are 15.95%, 41.37%, 17.72%, and 13.13%, respectively. An additional 11.83% of retrievals with QFlag $= 0$ or > 4 have been excluded. QFlag $= 2$ dominates across most levels, accounting for over 40% of retrievals from 825 hPa to 1 hPa, followed by QFlag values of 3, 1, and 4. For humidity profiles, the corresponding proportions are 14.99%, 45.81%, 15.33%, and 14.13%, respectively, with 9.74% of the data removed due to invalid QFlags. Similar to temperature, QFlag $=$ 2 shows the highest percentage, while the percentages for the other QFlags remain relatively balanced.

The dataset includes temperature and humidity profiles from surface (1000 hPa) to 1 hPa with 37 levels. The observations have a resolution of 14 km by 14 km at the surface. The data are available at the Chinese National Satellite Meteorological Center (NSMC, http://satellite.nsmc.org.cn/portalsite/Data/Satellite.aspx).

Due to the differences in humidity profiles between FY-3E (measured in g/kg) and radiosonde (measured in %), it is necessary to convert specific humidity (g/kg) to relative humidity (%) [18]:

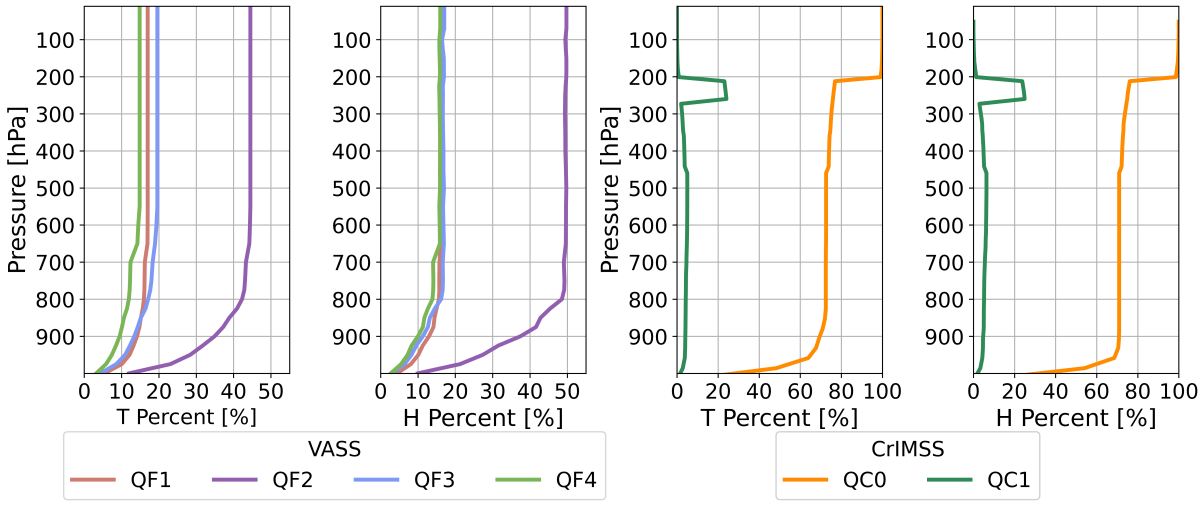

Fig. 1. The percentage of various quality flags for VASS, and CrIMSS temperature and humidity data used in this study.

$$e = \frac{q \cdot p}{0.622 + 0.378 \cdot q} \ , \tag{1}$$

$$es = \begin{cases} 6.112 \cdot \exp(\frac{17.67 \cdot (T - T_0)}{T - 29.65}) \ , & \text{if T >= 273.15} \\ 6.112 \cdot \exp(\frac{22.46 \cdot (T - T_0)}{T - 0.55}) \ , & \text{if T <273.15} \end{cases} \tag{2}$$

$$RH = \frac{e}{es} \cdot 100 \ , \tag{3}$$

where q is the specific humidity (unit: kg/kg), p is the pressure (unit: hPa), T is the temperature (unit: K), and T_0 = 273.15 K. e, es, and RH represent the water vapor pressure, saturated vapor pressure, and relative humidity (unit: %), respectively.

B. JPSS-1 CrIMSS products

The combination of the CrIS and ATMS, known as CrIMSS, has been onboard the Suomi-NPP since 2011, JPSS-1 since 2017, and JPSS-2 since 2022. The CrIS instrument is a Fourier transform spectrometer that features a total of 2,211 full spectral resolution infrared sounding channels. These channels encompass the long-wave (645–1,095 cm^{-1}), mid-wave (1,210–1,750 cm^{-1}), and short-wave (2,100–2,550 cm^{-1}) spectral regions. The ATMS instrument, on the other hand, is a cross-track scanner equipped with 22 channels that operate in spectral bands ranging from 23 GHz to 183 GHz.

The CrIMSS temperature and humidity products can be retrieved using the CLIMCAPS and NUCAPS algorithms, which employ a combination of infrared and microwave observations. Compared to the NUCAPS algorithm, CLIMCAPS reduces the propagation of scene-dependent spectral uncertainty by utilizing a priori estimates for temperature and water vapor that are largely independent of the spectral measurements [19]. This algorithm employs an Optical Estimation (OE) methodology and utilizes the second Modern-Era Retrospective analysis for Research and Applications (MERRA-2) as a priori first guess to retrieve temperature and humidity profiles [19], [20].

For both temperature and humidity products, the CrIMSS provides associated quality control (QC) indicators for each variable. QC = 0 indicates the 'best' retrievals that meet accuracy requirements, QC = 1 represents 'good' retrievals, and QC = 2 signifies that the use of such data is not recommended [4]. The percentages of various QCs for the CrIMSS temperature and humidity data used in this study are illustrated in Fig. 1. The percentage for QC = 0 is significantly higher than that for QC = 1 for both CrIMSS temperature and humidity data, approaching 100% from 200 hPa to 10 hPa. For the temperature profiles, the percentages for each QCs are approximately 84.80%, and 2.66%, respectively. Additionally, about 12.54% of the retrievals with QCs equal to 2 have been excluded. The percentage for temperature QC = 1 remains below 5% from 1000 hPa to 250 hPa, while it exceeds 23% between 250 hPa and 200 hPa. For the humidity profiles, the percentages for each QCs are approximately 76.37%, and 4.74%, respectively. Additionally, about 18.89% of the retrievals with QCs equal to 2 have been removed. The humidity QC = 1 percentage remains below 6.35% from 1000 hPa to 250 hPa and exceeds 23% from 250 hPa to 200 hPa.

The spatial resolution of this dataset is 50 km × 50 km, and the temporal coverage extends from February 17, 2018, to October 2, 2024 (data access date: December 7, 2024). The CrIMSS Level 2 product used in this paper is available at the NASA GES DISC [21].

The comparisons between the FY-3E VASS and the JPSS-1 CrIMSS are illustrated in Table I. The temperature and humidity profiles from the FY-3E VASS are retrieved using a neural network (PDNN), with ERA5 reanalysis data serving as the output training. In contrast, the temperature and humidity profiles from JPSS-1 CrIMSS are obtained through a physical algorithm (OE), utilizing MERRA-2 as the first-guess atmospheric state. The FY-3E VASS data is available in nearly real-time, whereas the CLIMCAPS-retrieved CrIMSS products typically experience a latency of about one month due to their dependence on MERRA-2 inputs that require post-processing and assimilation cycles [22].

TABLE I
THE COMPARISONS BETWEEN FY-3E VASS AND JPSS-1 CRIMSS.

Satellites	Date Time	a-priori (output training)	Algorithms	Retrieval Channels	Latency
FY-3E VASS	April 19, 2023 to August 31, 2024	ERA5	PDNN	450 channels from HIRAS, and all MWTS and MWHS channels	NRT
JPSS-1 CrIMSS	April 19, 2023 to August 31, 2024	MERRA-2	CLIMCAPS	IR channels from CrIS, and ATMS channels 3–15, 17-22	about 1-month delay [22]

C. FY4B GIIRS products

The Geostationary Interferometric Infrared Sounder (GIIRS) [23], onboard the FY-4B satellite launched in June 2021, provides hyperspectral infrared observations from geostationary orbit. It covers three spectral ranges: visible (0.55–0.90 μm), mid-infrared (1650–2250 cm^{-1}), and long-infrared (680–1130 cm^{-1}), with a spectral resolution of 0.8 cm^{-1}. The nadir spatial resolution is 1 km in the visible range and 12 km in the infrared, with a temporal resolution of 45 minutes. The Dual-Regression (DR) algorithm is currently employed as the operational algorithm by NSMC to produce temperature and humidity profiles from GIIRS measurements [24].

D. Radiosonde data

The Integrated Global Radiosonde Archive (IGRA), which contains meteorological records from radiosonde and pilot balloon observations, is maintained by the National Centers for Environmental Information (NCEI) of the National Oceanic Atmospheric Administration (NOAA). The IGRA2 radiosonde sounding dataset was released in 2016. Compared to IGRA1, IGRA2 expands its coverage by incorporating approximately 30 additional data sources, adding relative humidity as a variable alongside dewpoint depression, merging multiple datasets into a unique IGRA2 station record, and enhancing the quality assurance system [25]. Traditionally, radiosonde data has been utilized as a validation source for observations from other instruments and platforms [25]–[30].

Normally, the IGRA2 radiosonde station releases balloons twice daily, at 00:00 UTC and 12:00 UTC. Based on the spatiotemporal matching criteria (which will be illustrated in Sect. III-C), we utilized temperature and humidity profiles from a total of 496 radiosonde stations for this study, covering the period from April 19, 2023, to August 31, 2024, as shown in Fig. 2. The radiosonde stations compared with the VASS are primarily located in Asia, as well as in the central and southern regions of North America. In contrast, the radiosonde stations compared with the CrIMSS are predominantly situated in Europe. This distribution is attributable to the fact that both FY-3E and JPSS-1 are polar-orbiting satellites, along with the spatiotemporal matching criteria. During the release of sounding balloons, FY-3E monitors the atmosphere over Asia and North America, while JPSS-1 observes Europe, Africa, and North America.

III. METHODOLOGY

A. Data Preprocessing

Satellite data quality control primarily involves ensuring that the data is physically reasonable, applying quality flags, and eliminating outliers.

1) Physically Reasonable Cases: After data collection, physically unreasonable cases are discarded, including temperatures that exceed the range of −110°C to 50°C and relative humidity (RH) values that fall outside the range of 0% to 100% [31].

2) Quality Flag: According to the VASS QFlag (as detailed in Sect. II-A), we evaluate the VASS product under three conditions: clear sky (QFlag equals 1 or 2), cloudy sky (QFlag equals 3 or 4), and all-sky (QFlag equals 1, 2, 3, or 4). In the experiment, we select CrIMSS data that possess the 'best' or 'good' quality controls for further quality evaluation.

3) Elimination Outliers: The upper control limit of 3.0 sigma was used to identify and eliminate outliers. Within the same pressure level, if the temperature or relative humidity value exceeds the average by more than three times the standard deviation, it will be classified as an outlier and removed from the dataset.

$$\boldsymbol{x_{ij}} \in (\overline{\boldsymbol{x}}_{\boldsymbol{i}} - 3\boldsymbol{\sigma_i}, \overline{\boldsymbol{x}}_{\boldsymbol{i}} + 3\boldsymbol{\sigma_i}) \ , \tag{4}$$

where $\boldsymbol{x_{ij}}$ represents the temperature or relative humidity values for the j-th profile of the i-th pressure level that adheres to the three-sigma rule, $\overline{x}_i$ and σ_i denote the average temperature or relative humidity and the standard deviation of the i-th pressure level, respectively.

The VASS temperature and humidity products are provided on fixed pressure levels (37 levels between 1000 and 1 hPa). In the troposphere, the spacing of these pressure levels corresponds to an effective vertical sensitivity on the order of 1–2 km, as estimated from the pressure–height relationship, rather than from retrieval averaging kernels. This vertical scale is comparable in magnitude to the typical tropospheric vertical resolution reported for infrared and infrared-microwave sounding products, such as CrIS and CrIS/ATMS, which is commonly on the order of 1–2 km in the troposphere [32]–[34]. Radiosonde profiles have finer but irregular vertical spacing [35], so all RAOB temperature and humidity data were interpolated to the VASS (and CrIMSS) pressure levels, ensuring level-consistent evaluation. Because the retrieval uncertainty of VASS is generally larger than the expected smoothing mismatch between level- and layer-averaged quantities, the representativeness differences are expected to have only a minor impact on the validation results.

B. Statistical Metrics

The correlation coefficient (R) indicates the relationship between variables, while bias represents the difference between satellite products and radiosonde data. The root mean square error (RMSE) signifies the level of uncertainty. R, bias, and

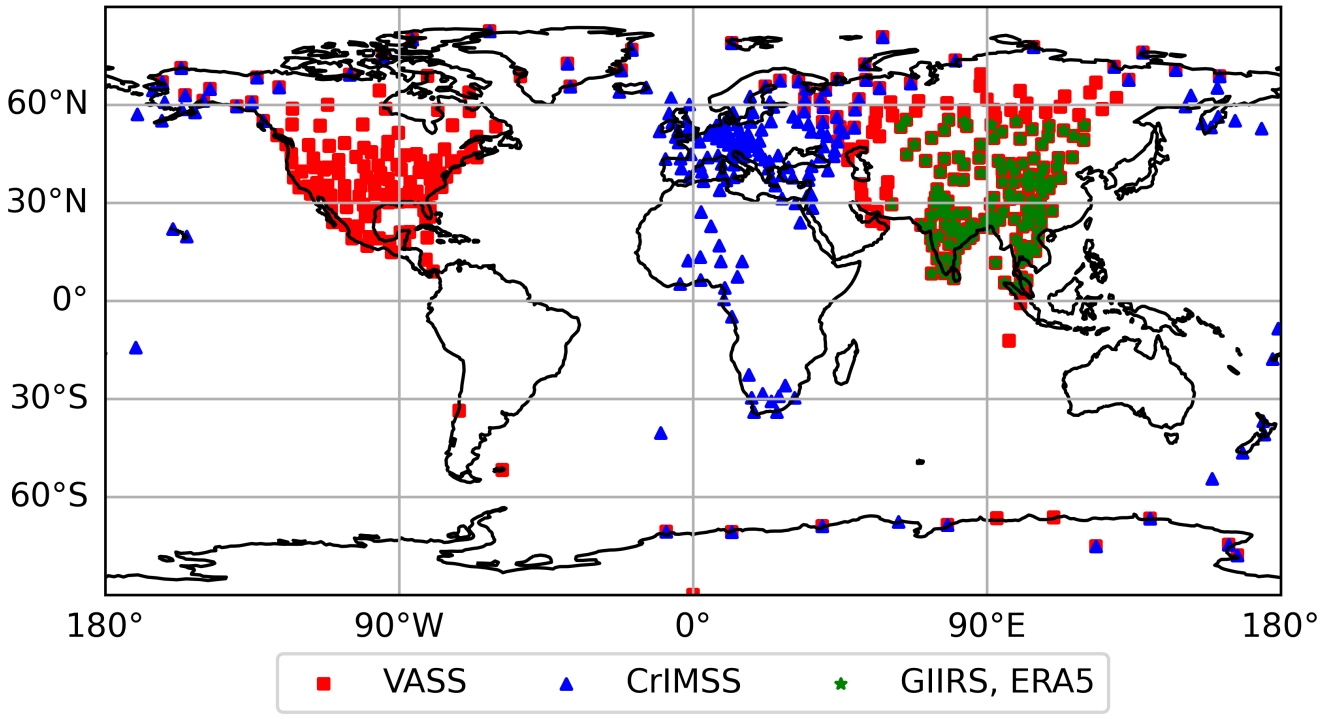

Fig. 2. Distribution of radiosonde stations utilized in this study. The red squares, totaling 351, represent the radiosonde stations used for comparison with the VASS profiles. The blue triangles, totaling 202, indicate the stations used for comparison with the CrIMSS profiles. The green stars, totaling 134, represent the stations used for comparison with the VASS, GIIRS, and ERA5 profiles.

RMSE were utilized to evaluate the discrepancies between satellite retrievals of temperature and humidity profiles and those obtained from radiosonde data. The equations are presented below:

$$\boldsymbol{R} = \frac{\sum_{i=1}^{n}(\boldsymbol{x_i} - \bar{\boldsymbol{x}})(\boldsymbol{y_i} - \bar{\boldsymbol{y}})}{\sqrt{\sum_{i=1}^{n}(\boldsymbol{x_i} - \bar{\boldsymbol{x}})^{\boldsymbol{2}} \sum_{i=1}^{n}(\boldsymbol{y_i} - \bar{\boldsymbol{y}})^{\boldsymbol{2}}}}, \tag{5}$$

$$\boldsymbol{bias} = \frac{\boldsymbol{1}}{\boldsymbol{n}} \sum_{i=1}^{n}(\boldsymbol{x_i} - \boldsymbol{y_i}), \tag{6}$$

$$\boldsymbol{RMSE} = \sqrt{\frac{\boldsymbol{1}}{\boldsymbol{n}} \sum_{i=1}^{n}(\boldsymbol{x_i} - \boldsymbol{y_i})^2}, \tag{7}$$

Where $\boldsymbol{x_i}$ represents the satellite temperature or humidity value, $\boldsymbol{y_i}$ denotes the radiosonde data, and n represents the number of samples, respectively.

C. Spatiotemporal Matching criteria

Divakarla et al. [36] employed a temporal window of ±3 hours and a spatial radius of 100 km for collocating radiosonde (RAOB) measurements with AIRS observations. He et al. [31] adopted a 1-hour temporal window and a 50 km spatial threshold to validate observations from FY-4A. Zhang et al. [37] used stricter criteria—within 30 minutes and 0.1°—for matching MWTHS data with ERA5 and NCEP. Fan et al. [38] selected 90 minutes and 100 km as the temporal and spatial windows for data matching.

To assess the impact of collocation thresholds on the validation results, a sensitivity analysis was carried out over China using three spatiotemporal criteria: (2 h, 1°), (1 h, 0.5°), and (0.5 h, 0.25°), as shown in Figs. S3-S4 and Table S1. The results indicate that the overall vertical error structures are consistent across the three thresholds. However, using a relatively loose criterion (2 h, 1°) leads to a noticeable increase in RMSE, particularly between 600 and 200 hPa. Further tightening the thresholds beyond (1 h, 0.5°) results in only marginal improvements, which can be attributed to the horizontal drift of radiosonde balloons during ascent, typically on the order of 50 km.

In this study, a temporal threshold of 1 hour and a spatial collocation criterion of 0.5°are applied to match radiosonde observations with the FY-3E VASS, JPSS-1 CrIMSS, FY-4B GIIRS, and ERA5 datasets. Considering both statistical behavior and physical representativeness, this choice provides a reasonable and physically meaningful compromise for collocating satellite and radiosonde observations.

IV. Results and Discussion

This section evaluates the performance of the FY-3E VASS temperature and humidity retrievals against radiosonde observations from April 2023 to August 2024. Section IV-A presents the global and zonal-scale comparisons of VASS and CrIMSS temperature and humidity products, including bias and RMSE metrics. Section IV-B focuses on the retrieval accuracy of VASS temperature profiles over the Tibetan Plateau. Further intercomparisons among VASS, CrIMSS, GIIRS, and ERA5

using collocated radiosonde observations are presented in Section IV-C. All reported mean bias and RMSE values are calculated over the pressure range from 1000 hPa to 10 hPa. Here, the mean bias refers to the mean absolute bias.

A. *Comparison between VASS and CrIMSS using radiosonde data*

Fig. 3 presents density scatterplots comparing temperature retrievals from FY-3E VASS and JPSS-1 CrIMSS with collocated radiosonde observations. Both VASS and CrIMSS temperature exhibit strong agreement with radiosonde measurements, with correlation coefficients reaching 0.99 for VASS under clear-sky, cloudy-sky, and all-sky conditions. CrIMSS temperature retrievals show correlations of 1.00 across retrievals classified as best, good, and either best or good. Fig. 4 shows similar comparisons for humidity profiles. VASS humidity retrievals yield correlation coefficients of 0.78, 0.77, and 0.77 under clear-sky, cloudy-sky, and all-sky conditions, respectively. CrIMSS humidity retrievals exhibit slightly higher correlations, indicating a better agreement with radiosonde data. The correlation coefficients for VASS humidity retrievals in the lower troposphere (0.58, 0.44, and 0.54) and mid troposphere (0.52, 0.46, and 0.52) are slightly higher than those in the upper troposphere (0.45, 0.41, and 0.47), whereas for CrIMSS, the correlation coefficients exhibit the opposite trend (see Figs. S1 and S2). For both VASS and CrIMSS humidity retrievals, the correlation coefficients for the entire atmosphere are higher compared to those for the individual tropospheric layers. The temperature retrievals from both VASS and CrIMSS demonstrate excellent consistency with radiosonde data, with correlation coefficients close to 1.0. Although VASS humidity retrievals show slightly weaker correlations compared to CrIMSS, they still achieve a reliable performance with correlations close to 0.80.

Figure 5 presents the vertical distributions of bias and RMSE for temperature (left panels) and humidity (right panels) profiles retrieved from FY-3E VASS (QFlag = 1) and JPSS-1 CrIMSS (QC = 0), using collocated radiosonde data as reference. The VASS temperature profiles show higher biases and RMSEs than CrIMSS at the majority of pressure levels. Quantitatively, the mean bias and RMSE of VASS are 0.59 K and 2.98 K, respectively, while CrIMSS has a mean bias of 0.07 K and an RMSE of 1.32 K. Despite these differences, VASS temperature profiles maintain a good agreement with radiosonde data across a wide range of altitudes. For humidity, the comparison shows more complex variability. VASS humidity retrievals exhibit lower bias than CrIMSS at several pressure ranges (950–900 hPa, 700–550 hPa, 400–350 hPa, and 125–100 hPa), whereas CrIMSS performs better at other levels. The RMSE values for VASS humidity profiles are generally higher than thoese of CrIMSS in the lower and mid-troposphere (1000–150 hPa), but are marginally lower at high altitudes (above 125 hPa). The mean bias and RMSE of VASS are 5.93% (2.46%, 1.92%, and 16.57% for the lower, mid, and upper troposphere, respectively) and 18.92% (20.65%, 23.81%, and 29.46%), while CrIMSS achieves 5.23% (1.74%, 3.22%, and 14.10%) and 16.17% (15.07%, 17.72%, and 20.86%) for the same levels. These results suggest that although CrIMSS outperforms in overall accuracy, VASS provides reasonable performance and is able to capture key vertical structures of atmospheric humidity, especially at high altitudes (above 125 hPa). This supports its potential for operational monitoring and data assimilation applications.

Fig. 6 shows the bias and RMSE of temperature and humidity profiles retrieved from VASS (under different sky conditions) and CrIMSS (with different quality flags), using radiosonde observations as reference. Compared to radiosonde data, the FY-3E VASS temperature products slightly underestimate temperature values between 900 hPa and 100 hPa, while overestimating temperatures at altitudes both below 900 hPa and above 100 hPa. The mean biases of VASS are 0.63 K (clear sky), 0.82 K (cloudy sky), and 0.67 K (all-sky). The RMSEs remain below 3.00 K above 700 hPa under clear sky and below 4.00 K above 650 hPa under cloudy sky. The corresponding mean RMSEs are 3.07 K, 3.56 K, and 3.26 K, respectively. In comparison, CrIMSS temperature retrievals show smaller biases, mostly within ±0.5 K. For best retrievals, the mean bias and RMSE are 0.07 K and 1.32 K, respectively. For good retrievals, they are 0.24 K and 1.41 K, and for either best or good retrievals, 0.07 K and 1.33 K. The VASS humidity bias remains within ±5% from 975 hPa to 500 hPa and above 150 hPa. Similarly, under cloudy-sky conditions, the bias stays within ±5% from 900 hPa to 600 hPa and above 175 hPa. The mean VASS humidity biases are 4.63% (clear sky), 6.21% (cloudy sky), and 4.76% (all-sky), with respective breakdowns across the lower, mid, and upper troposphere of (0.79%, 0.46%, 13.42%), (−2.71%, 5.61%, 16.74%), and (−0.22%, 2.11%, 14.43%). The VASS humidity RMSEs exceed 20% below 150 hPa but remain below 10% at higher altitudes. The mean RMSEs are 18.36% (20.91%, 23.93%, and 27.61% for the lower, mid, and upper troposphere, respectively), 21.38% (23.93%, 27.79%, and 32.48%), and 19.36% (21.85%, 25.23%, and 29.19%) for clear, cloudy, and all-sky conditions, respectively. For CrIMSS, humidity profile biases for best retrievals are mostly within ±10%, and within ±15% for good retrievals, with exceptions at specific levels. The mean biases are 5.23% (1.74%, 3.22%, 14.10% for the lower, mid, and upper troposphere, respectively) for best retrievals, 0.93% (−3.16%, −1.26%, 6.98%) for good retrievals, and 4.94% (1.42%, 2.88%, 13.54%) for either best or good. The RMSEs for CrIMSS best humidity retrievals are generally below 20%, and slightly higher for good retrievals. The mean RMSEs are 16.17% (15.07%, 17.72%, and 20.86% for the lower, mid, and upper troposphere, respectively), 17.63% (15.08%, 18.45%, and 19.84%), and 16.19% (15.10%, 17.77%, and 20.74%) for best, good, and combined categories, respectively. More details regarding the bias and RMSE of the FY-3E VASS and JPSS-1 CrIMSS products at different pressure levels, as compared with radiosonde data, are presented in Table II.

Although both satellite datasets provide global observations, the collocated profiles used for ground-based validation in this study are unevenly distributed. As shown in Fig. 2, the radiosonde matchups used for VASS and CrIMSS are not globally coincident. The CrIMSS profiles are mostly distributed over Europe, with some coverage in Africa, whereas

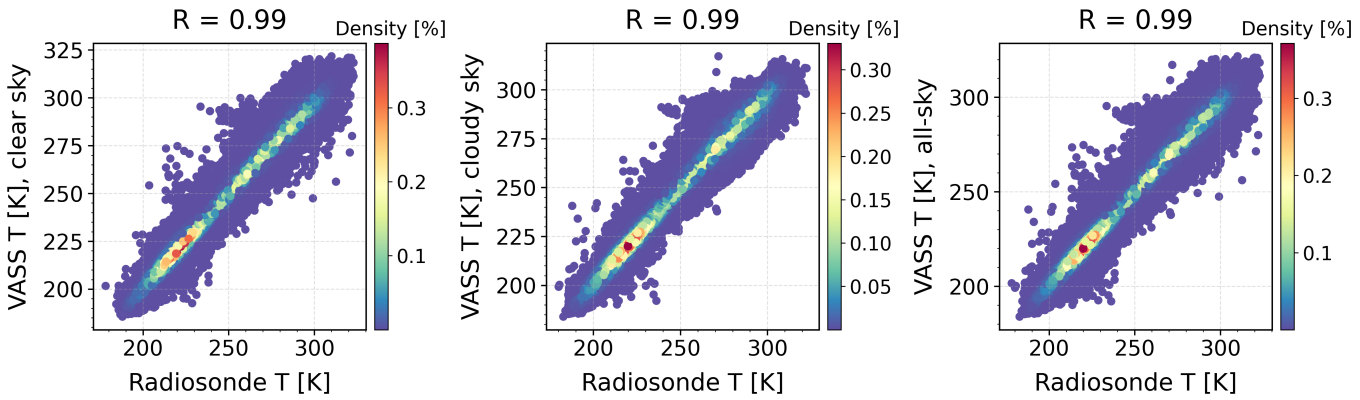

(a) FY-3E VASS (clear sky, cloudy sky, and all-sky conditions)

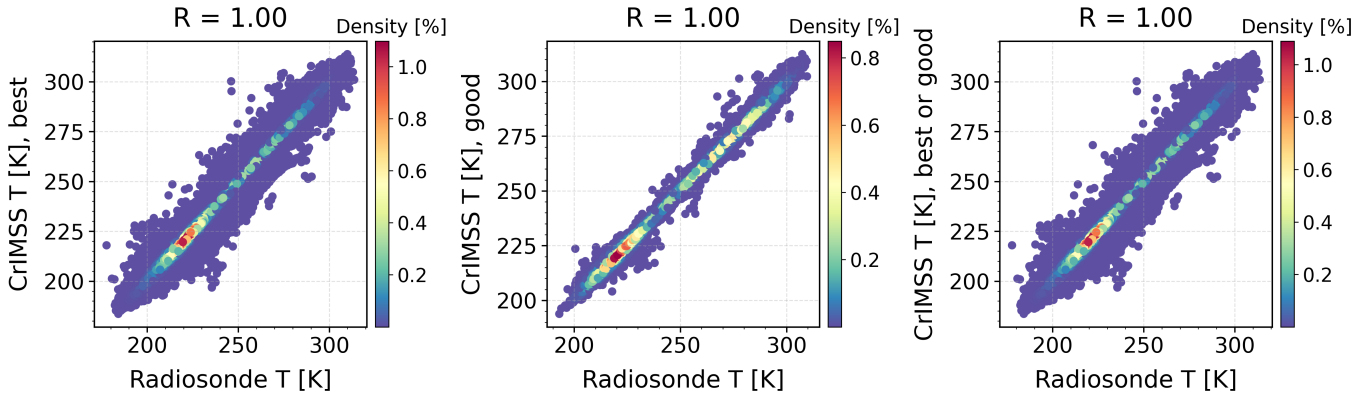

(b) JPSS-1 CrIMSS (the best, good, and either the best or good)

Fig. 3. The density of scatterplots compares (a) the clear sky, cloudy sky, and all-sky conditions flagged samples of FY-3E VASS temperature products to radiosonde data, and (b) the best, good, and either the best or good flagged samples of JPSS-1 CrIMSS temperature products to radiosonde data. The density represents the percentage of samples in relation to the total number of samples.

the VASS profiles are concentrated in Asia, including the Qinghai–Tibet Plateau, and in North America covering both eastern and western mountainous regions. Radiosonde stations in these regions also use different instruments [39]. Previous evaluations of global reanalysis products reported the largest RMSEs in North America and the smallest in Europe [40]. COSMIC temperature and humidity profiles also show large RMSEs over the Indian subcontinent, China, and North America when compared with radiosonde data [39]. These geographic, topographic, and instrumental differences may contribute to the discrepancies observed between VASS and CrIMSS products. Therefore, the results mainly reflect the performance in these regions and should not be interpreted as representative of the global situation.

Fig. 7 presents the bias and RMSE of FY-3E VASS and CrIMSS temperature profiles across five latitude zones: 90°S–60°S, 60°S–20°S, 20°S–20°N, 20°N–60°N, and 60°N–90°N. Compared to radiosonde measurements, VASS temperature retrievals exhibit a systematic cold bias in the low-latitude region (20°S–20°N), particularly between 1000 hPa and 600 hPa. Across all latitude zones, the VASS temperature bias between 600 hPa and 300 hPa remains relatively small, especially under clear-sky conditions where it ranges from −0.61 K to 0.19 K. This indicates that VASS maintains consistent accuracy in the mid-troposphere globally. In terms of RMSE, VASS temperature profiles show lower errors in the tropics (20°S–20°N) below 150 hPa compared to higher-latitude regions (90°S–60°S, 20°N–60°N, and 60°N–90°N), suggesting better retrieval performance in the tropics. Under clear sky conditions, the RMSE in the 60°S–20°S region is slightly lower than those in the 20°S–20°N region between 825 hPa and 600 hPa. For CrIMSS temperature, the bias of the best and combined best/good retrievals is generally consistent across all latitude zones, particularly between 90°S and 60°S. This is likely due to the predominance of best-retrieval pixels in this region. In mid- and high-latitude zones (90°S–20°S and 20°N–90°N), the CrIMSS temperature bias remains within ±0.5 K from 800 hPa to 100 hPa, demonstrating stable performance across a broad vertical range. The RMSEs in the tropics are within 2 K (except at 125 hPa) and are lower than those in other latitude zones. Overall, CrIMSS temperature retrievals outperform VASS across latitude zones. VASS, however, shows reasonable performance in the mid-troposphere and tropics. Further refinement of its algorithm, particularly for high latitudes and near-surface layers, is needed to improve the retrieval accuracy.

Fig. 8 depicts the bias and RMSE of the VASS and CrIMSS humidity profiles across three latitude zones. For VASS hu-

TABLE II

BIAS AND RMSE FOR THE FY-3E VASS AND JPSS-1 CRIMSS PRODUCTS COMPARED TO COLLOCATED RADIOSONDE DATA.

Pressure	VASS T bias [K]			CrIMSS T bias [K]			VASS T RMSE [K]			CrIMSS T RMSE [K]			VASS H bias [%]			CrIMSS H bias [%]			VASS H RMSE [%]			CrIMSS H RMSE [%]		
	clear	cloudy	all-sky	best	good	best or good	clear	cloudy	all-sky	best	good	best or good	clear	cloudy	all-sky	best	good	best or good	clear	cloudy	all-sky	best	good	best or good
1000	2.15	0.98	1.81	0.00	0.35	0.02	5.57	4.92	5.39	1.67	1.49	1.66	−5.50	−11.79	−7.27	0.68	−1.52	0.50	19.18	22.57	20.20	10.69	10.30	10.63
975	1.35	0.09	0.96	−0.16	0.45	−0.13	5.63	5.32	5.54	2.33	2.42	2.34	−2.70	−9.24	−4.57	2.04	−2.65	1.76	20.59	23.76	21.55	12.23	9.17	12.05
950	0.65	−0.24	0.38	−0.05	0.48	−0.02	4.99	5.11	5.03	1.97	2.29	2.00	−1.04	−7.92	−3.04	3.77	−2.86	3.39	20.46	23.55	21.41	12.97	9.53	12.81
925	0.29	−0.37	0.08	−0.01	0.31	0.01	4.39	4.71	4.49	1.38	1.70	1.40	−0.60	−7.34	−2.56	3.59	−0.91	3.32	20.02	23.78	21.18	12.40	9.37	12.31
900	−0.23	−0.63	−0.36	−0.04	0.20	−0.03	4.23	4.87	4.44	1.55	1.69	1.56	1.08	−4.65	−0.61	3.92	0.28	3.69	20.11	23.32	21.11	14.05	10.85	13.88
875	−0.62	−1.06	−0.76	−0.07	0.11	−0.06	4.04	4.93	4.34	1.50	1.69	1.52	2.11	−1.83	0.94	1.99	−2.61	1.67	20.46	23.31	21.34	14.38	12.84	14.36
850	−0.90	−1.33	−1.04	−0.06	0.03	−0.06	3.70	4.91	4.13	1.07	1.22	1.08	2.69	−0.98	1.59	−0.15	−6.07	−0.56	21.05	23.85	21.93	15.40	16.15	15.44
825	−1.08	−1.71	−1.29	0.00	0.05	0.00	3.86	5.33	4.40	1.42	1.43	1.43	3.03	1.20	2.47	0.54	−6.79	0.11	21.56	24.11	22.37	17.74	22.93	18.06
800	−1.24	−1.97	−1.48	−0.01	−0.04	−0.01	3.87	5.67	4.55	1.55	1.58	1.55	3.49	3.52	3.50	0.54	−5.89	0.10	21.81	24.59	22.72	19.09	21.73	19.28
775	−1.30	−2.19	−1.60	−0.02	−0.15	−0.02	3.70	5.54	4.40	1.52	1.55	1.53	3.34	4.53	3.71	0.91	−3.64	0.59	22.34	25.13	23.26	18.52	21.40	18.74
750	−1.32	−2.13	−1.59	−0.01	−0.14	−0.01	3.48	5.22	4.15	1.42	1.42	1.42	2.81	4.69	3.41	1.30	−2.08	1.06	22.41	25.25	23.34	18.31	21.56	18.56
700	−1.14	−2.11	−1.47	−0.02	−0.12	−0.03	2.87	4.74	3.62	0.86	0.92	0.86	−0.34	3.66	0.91	2.09	−2.27	1.76	23.11	25.71	23.95	17.10	20.23	17.35
650	−0.61	−1.36	−0.88	0.04	−0.05	0.03	2.56	3.23	2.81	1.26	1.23	1.26	−2.58	4.35	−0.33	1.71	−0.92	1.52	23.60	25.71	24.30	17.35	17.05	17.33
600	−0.37	−1.10	−0.63	0.04	0.04	0.04	2.41	2.93	2.61	1.29	1.35	1.29	−3.53	4.12	−1.07	1.95	−0.52	1.77	24.08	26.86	25.01	17.58	17.85	17.60
550	−0.32	−0.72	−0.46	0.05	0.16	0.06	2.30	2.63	2.42	1.16	1.29	1.17	−1.24	5.46	0.89	2.86	−0.01	2.63	23.93	28.83	25.60	17.88	18.53	17.93
500	−0.28	−0.40	−0.32	0.06	0.24	0.07	2.12	2.32	2.19	0.81	0.88	0.81	4.11	6.19	4.78	4.42	−1.43	3.96	24.20	29.31	25.95	17.29	19.11	17.45
450	−0.40	−0.28	−0.36	0.04	0.33	0.05	2.26	2.45	2.33	1.12	1.23	1.13	6.36	9.89	7.48	6.27	−2.41	5.67	24.68	30.29	26.59	19.11	17.92	18.96
400	−0.41	−0.22	−0.35	0.01	0.28	0.02	2.11	2.31	2.18	0.81	0.99	0.82	7.26	12.49	8.89	9.92	0.29	9.29	24.36	30.97	26.60	19.45	17.70	19.33
350	−0.46	−0.30	−0.40	0.11	0.39	0.12	2.28	2.50	2.36	1.15	1.22	1.16	9.30	15.84	11.28	12.29	2.11	11.68	25.43	32.49	27.75	20.72	21.60	20.80
300	−0.50	−0.36	−0.45	0.05	0.38	0.06	2.11	2.52	2.26	0.86	0.99	0.86	14.72	18.92	15.97	16.40	4.68	15.84	28.70	33.56	30.22	21.87	19.52	21.75
250	−0.24	−0.39	−0.30	0.20	0.49	0.27	2.58	2.86	2.68	1.04	1.32	1.10	18.72	19.02	18.81	16.89	14.90	16.36	30.82	33.36	31.58	21.58	21.26	21.48
225	0.06	−0.27	−0.06	0.22	0.44	0.27	3.04	3.21	3.10	1.46	1.72	1.52	17.10	17.41	17.19	14.99	12.90	14.51	28.76	32.04	29.78	20.66	19.15	20.32
200	0.35	−0.26	0.13	0.29	0.30	0.30	2.81	3.10	2.92	1.23	1.26	1.23	10.64	11.49	10.91	9.24	6.95	9.28	21.39	28.10	23.74	14.64	25.43	14.75
175	0.24	−0.45	−0.01	−0.04	0.16	−0.04	2.78	3.12	2.91	1.77	1.47	1.77	5.72	4.21	5.22	6.87	2.98	6.97	15.92	22.74	18.47	12.37	18.79	12.52
150	−0.10	−0.78	−0.34	0.00	−0.29	0.00	2.25	2.65	2.40	1.05	0.93	1.05	4.37	0.92	3.23	6.15	20.78	6.18	12.54	15.29	13.51	12.96	20.92	13.00
125	−0.25	−0.64	−0.39	−0.04	−0.38	−0.04	2.49	2.81	2.61	1.84	1.31	1.84	3.69	0.18	2.54	6.36	–	6.38	8.90	9.80	9.21	14.20	–	14.22
100	−0.54	−0.51	−0.53	−0.11	–	−0.11	2.22	2.38	2.27	0.99	–	0.99	3.95	1.55	3.16	6.32	–	6.34	7.56	6.58	7.26	15.20	–	15.21
70	0.27	0.46	0.34	−0.11	–	−0.11	2.43	2.35	2.41	1.05	–	1.05	2.11	1.38	1.87	2.57	–	2.58	3.65	3.14	3.49	7.05	–	7.08
50	0.88	0.97	0.91	−0.05	–	−0.05	2.18	2.24	2.20	1.05	–	1.05	0.12	−0.01	0.08	–	–	–	0.98	1.14	1.04	–	–	–
30	0.77	0.55	0.70	0.03	–	0.03	2.14	2.11	2.13	1.14	–	1.14	−0.99	−1.03	−1.00	–	–	–	1.33	1.39	1.35	–	–	–
20	0.18	−0.09	0.09	0.12	–	0.12	2.17	2.16	2.17	1.28	–	1.28	−1.34	−1.37	−1.35	–	–	–	1.64	1.70	1.66	–	–	–
10	0.71	1.23	0.89	−0.10	–	−0.10	2.69	2.82	2.73	1.63	–	1.63	−1.58	−1.65	−1.61	–	–	–	1.90	1.98	1.93	–	–	–

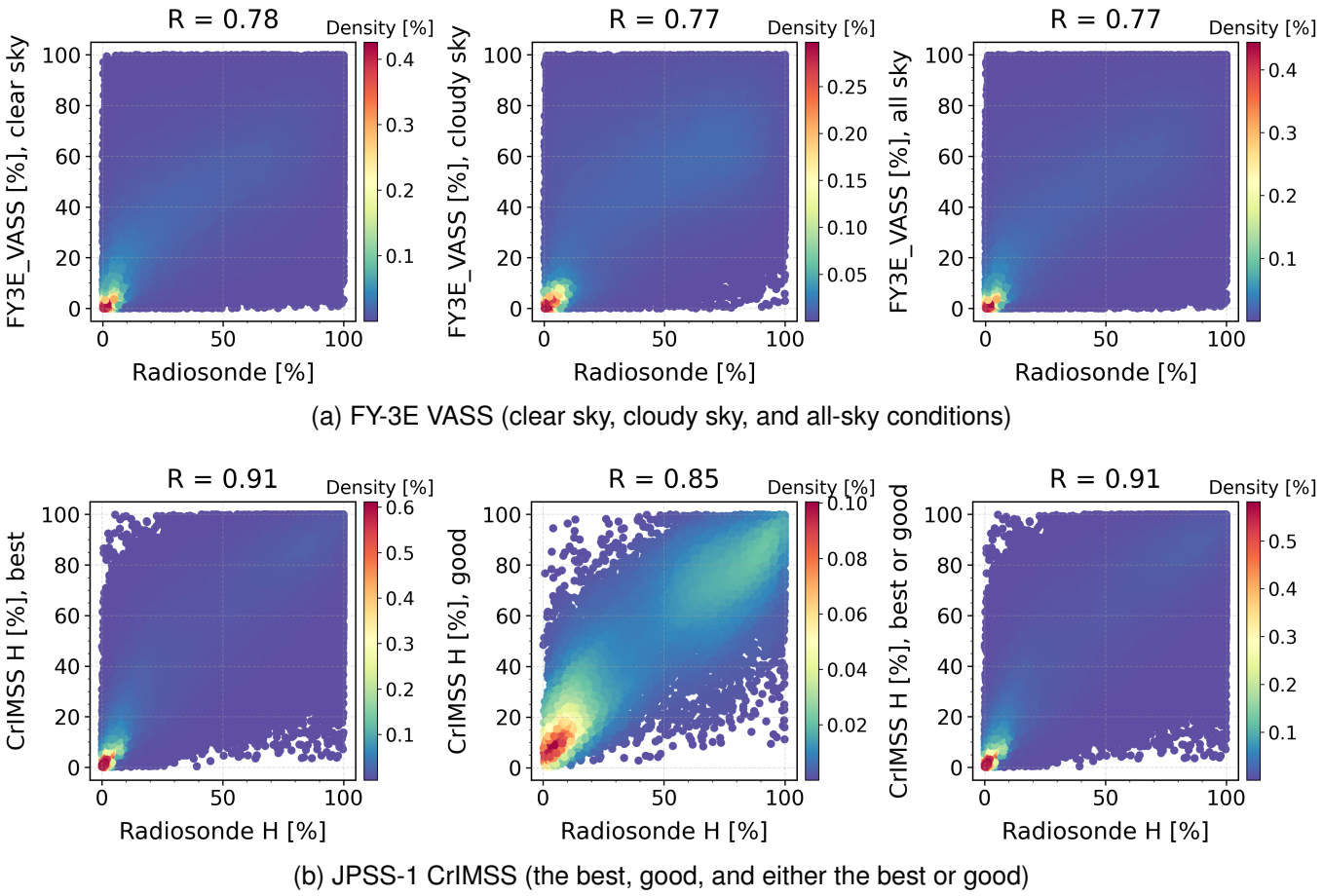

Fig. 4. Same as Fig. 3, but for humidity.

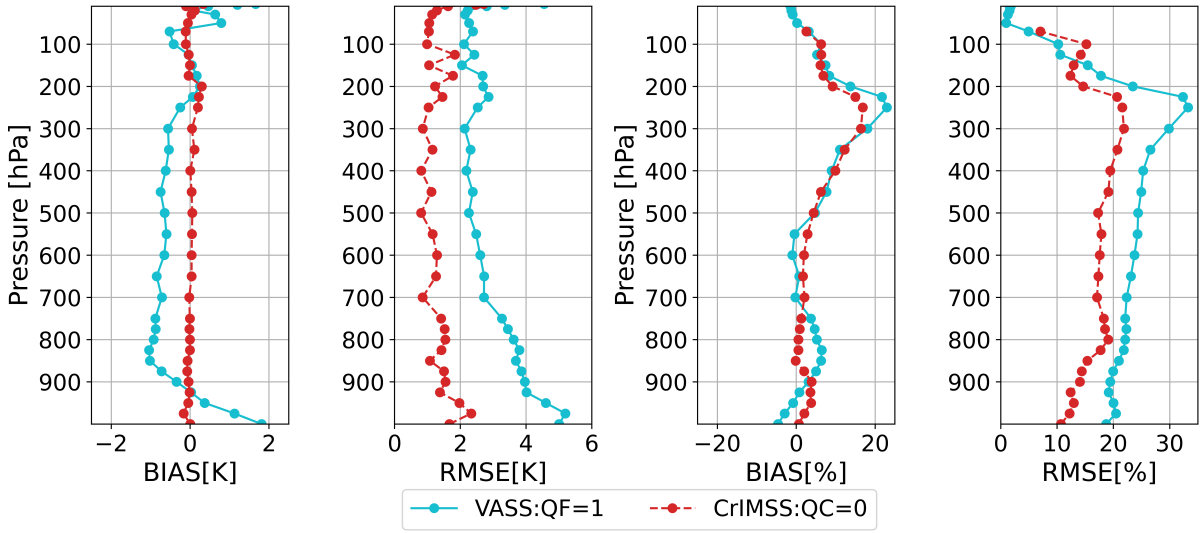

Fig. 5. Bias and RMSE for temperature and humidity profiles from FY-3E VASS (QFlag = 1; solid cyan lines) and JPSS-1 CrIMSS (QC = 0; red dashed lines), as compared to collocated radiosonde observations. Left panels show temperature results; right panels show humidity results.

midity, the bias values under both clear and all-sky conditions remain consistent across all latitude zones below 700 hPa. In the 20°S–20°N region, the bias is notably lower between 550 hPa and 300 hPa, while in the 60°N–90°N region, it is smaller than in other zones from 250 hPa to 50 hPa. Regarding RMSE, VASS humidity retrievals in the 20°S–20°N zone show lower errors compared to higher latitudes, especially within 1000 hPa to 800 hPa. Above 300 hPa, the RMSE in the 60°N–90°N zone is also lower than in the other latitude bands. These results indicate that VASS maintains relatively stable

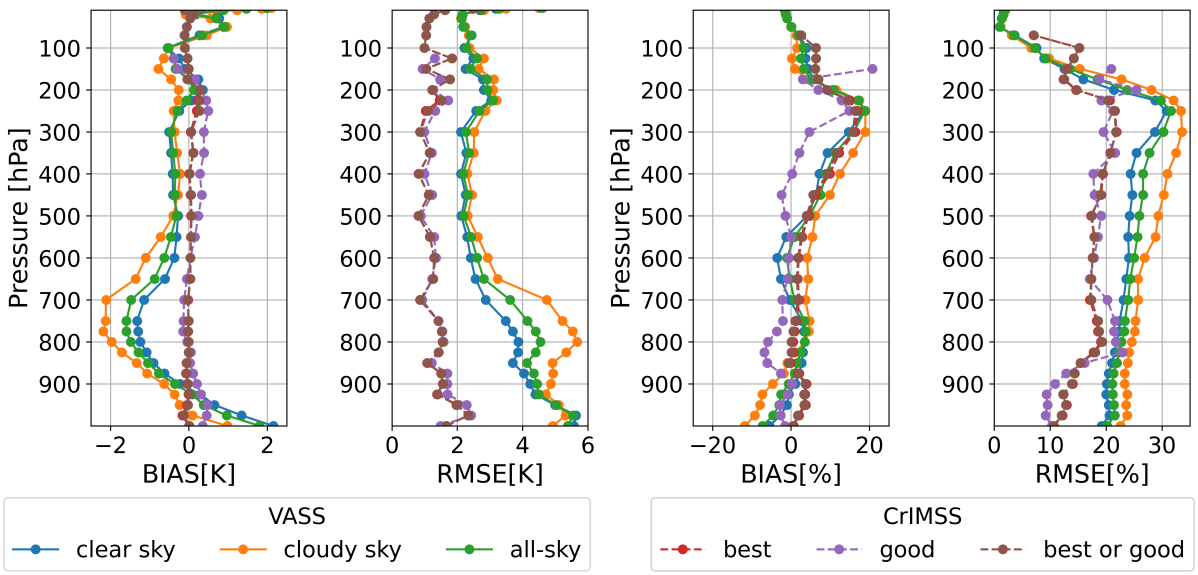

Fig. 6. Same as Fig. 5. The solid lines in blue, orange, and green represent VASS products under clear-sky, cloudy-sky, and all-sky conditions, respectively, while the dashed lines in red, purple, and brown represent CrIMSS products with QCs for the best, good, and combined best/good retrievals, respectively.

humidity performance across different regions and performs particularly well in the tropics and polar upper troposphere. For CrIMSS humidity, the bias of good retrievals is generally lower than those of the best or combined retrievals between 500 hPa and 200 hPa in all three zones. In terms of RMSE, CrIMSS performs well between 1000 hPa and 800 hPa, with values remaining within 20% in the 20°S–60°N zone. It can be seen that the humidity bias of VASS is comparable to that of CrIMSS under both clear- and all-sky conditions. Although the VASS RMSE is higher than CrIMSS at lower and mid-tropospheric levels, it is similar or even slightly better at upper levels (above 200 hPa), supporting the reliability of VASS humidity retrievals in diverse atmospheric environments.

B. Region validation of VASS temperature profiles over the Tibetan Plateau

The Tibetan Plateau spans from 26°00′12″N to 39°46′50″N and from 73°18′52″E to 104°46′59″E [41], covering an area of approximately 2.5 million km^2 with an average elevation exceeding 4.5 km [42]. The Plateau is characterized by its high elevation, thin atmosphere, complex topography, and fragile ecosystem, which plays a vital role in modulating atmospheric circulation and influencing weather and climate over Asia and globally. Therefore, achieving accurate measurements of atmospheric temperature and humidity over this region is of great importance. In this study,the performance of the FY-3E VASS products over the Tibetan Plateau has been evaluated through comparison with radiosonde observations. Using spatiotemporal matching criteria—specifically, a time window of ±1 hour and a spatial threshold of 0.5°—we identified eleven radiosonde stations within the region (see Fig. 2), yielding a total of 1,804 matched data pairs for analysis. The analysis is subject to the following conditions: (1) No CrIMSS and radiosonde observations simultaneously satisfy the matching criteria over the Tibetan Plateau; therefore, the analysis in this section focuses solely on comparisons between the VASS and radiosonde data. (2) Due to the absence of radiosonde humidity data from April 19, 2023, to August 31, 2024, the evaluation is limited to temperature profile comparisons. (3) Given the high terrain of the Tibetan Plateau, the surface elevations of the selected radiosonde stations exceed 1.5 km, resulting in radiosonde temperature measurements being primarily available above 775 hPa.

Fig. 9 illustrates the bias and RMSE of VASS temperature profiles in comparison to radiosonde observations over the Tibetan Plateau. The mean bias of temperature is −1.16 K under clear sky, −1.28 K under cloudy sky, and −1.22 K under all-sky conditions. The mean RMSE of temperature is 2.71 K under clear sky, 3.04 K under cloudy sky, and 2.94 K under all-sky conditions. Compared to the 20°N to 60°N zone, the bias values of VASS temperature over the Tibetan Plateau are higher under the same conditions from 700 hPa to 100 hPa, and the bias values are comparable between 100 hPa and 1 hPa. Under clear sky conditions, the RMSE values over the Tibetan Plateau are higher than those in the 20°N to 60°N zone within the pressure ranges of 750 hPa to 450 hPa, and 200 hPa to 150 hPa. Under cloudy sky conditions, the RMSE values over the Tibetan Plateau are higher than those in the 20°N to 60°N zone across the ranges of 700 hPa to 450 hPa, 350 hPa to 250 hPa, and 200 hPa to 70 hPa. Under all-sky conditions, the RMSE values are higher than those observed in the 20°N to 60°N zone, except at 775 hPa, 750 hPa, 225 hPa, and above 70 hPa. Compared to the global region (as shown in Fig. 6, the biases over the Tibetan Plateau are greater under the same conditions within the pressure range of 700 hPa to 100 hPa. The RMSE of temperature is higher in the range of 700 hPa to 500 hPa. At other pressure levels, the RMSE values for the two regions are comparable.

Due to the unique terrain of the Tibetan Plateau, which is characterized by its high altitude, accurately retrieving

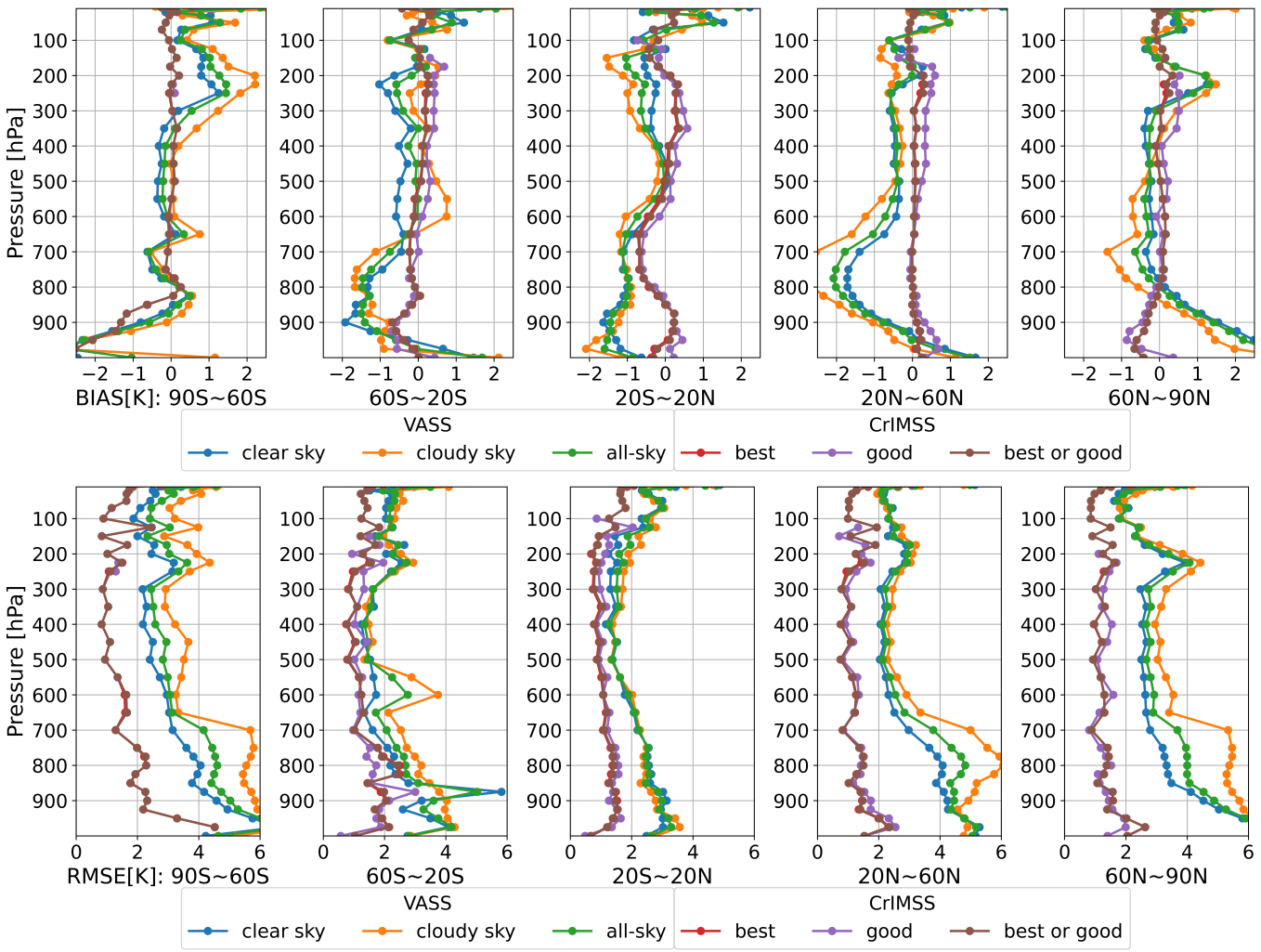

Fig. 7. Bias and RMSE of the VASS and CrIMSS temperature profiles across various latitude zones. The blue, orange, and green solid lines represent clear sky, cloudy sky, and all-sky conditions, respectively, while the red, purple, and brown solid lines represent CrIMSS products with the best, good, and either the best or good retrievals.

atmospheric components such as temperature, humidity, and other factors presents significant challenges. Compared to the neighboring latitude zones, the discrepancy between VASS and radiosonde observations is notably more pronounced. However, VASS temperature and humidity profiles are obtained by integrating infrared and microwave spectra, allowing for continuous and uninterrupted measurements over the Tibetan Plateau, even in cloudy conditions or at night.

C. Comparison between VASS and other products using coincident radiosonde data

To reduce the influence of heterogeneous radiosonde accuracy and terrain-induced evaluation challenges, this study selects 57 radiosonde stations with coincident observations for both VASS and CrIMSS, and 134 stations with coincident observations for VASS, GIIRS, and ERA5, as shown in Fig. 2. Fig. 10 shows the bias and RMSE of the VASS and CrIMSS temperature and humidity profiles in comparison with the coincident radiosonde data. The VASS temperature profiles under all-sky conditions exhibit bias values within ±0.9 K from 875 hPa to 300 hPa. The cloudy-sky retrievals show slightly smaller biases than those under clear or all-sky conditions at both lower (1000–825 hPa) and upper (450–350 hPa) tropospheric levels. The mean temperature bias for VASS is 0.76 K (clear sky), 0.74 K (cloudy sky), and 0.73 K (all-sky). CrIMSS temperature retrievals also perform well, with biases generally within ±1 K, and mean biases of −0.06 K (best), 0.01 K (good), and −0.06 K (combined). In terms of RMSE, VASS temperature retrievals stay below 4,K, except near the surface and upper stratosphere, with average values of 3.31 K (clear), 4.12 K (cloudy), and 3.58 K (all-sky). CrIMSS achieves lower RMSEs (typically below 2 K), with mean values of 1.37 K (best), 1.03 K (good), and 1.37 K (combined).

For humidity, VASS shows smaller biases than CrIMSS (best/good), specifically in the ranges of 975–700 hPa, 600–550 hPa, and 300–125 hPa. The mean bias of VASS humidity is 4.31% under clear-sky conditions (−0.08%, 5.38%, and 14.50% in the lower, mid, and upper troposphere), 4.23% under cloudy sky (−1.45%, 5.06%, and 14.96%), and 4.23% under all-sky conditions (−0.53%, 5.28%, and 14.67%). By

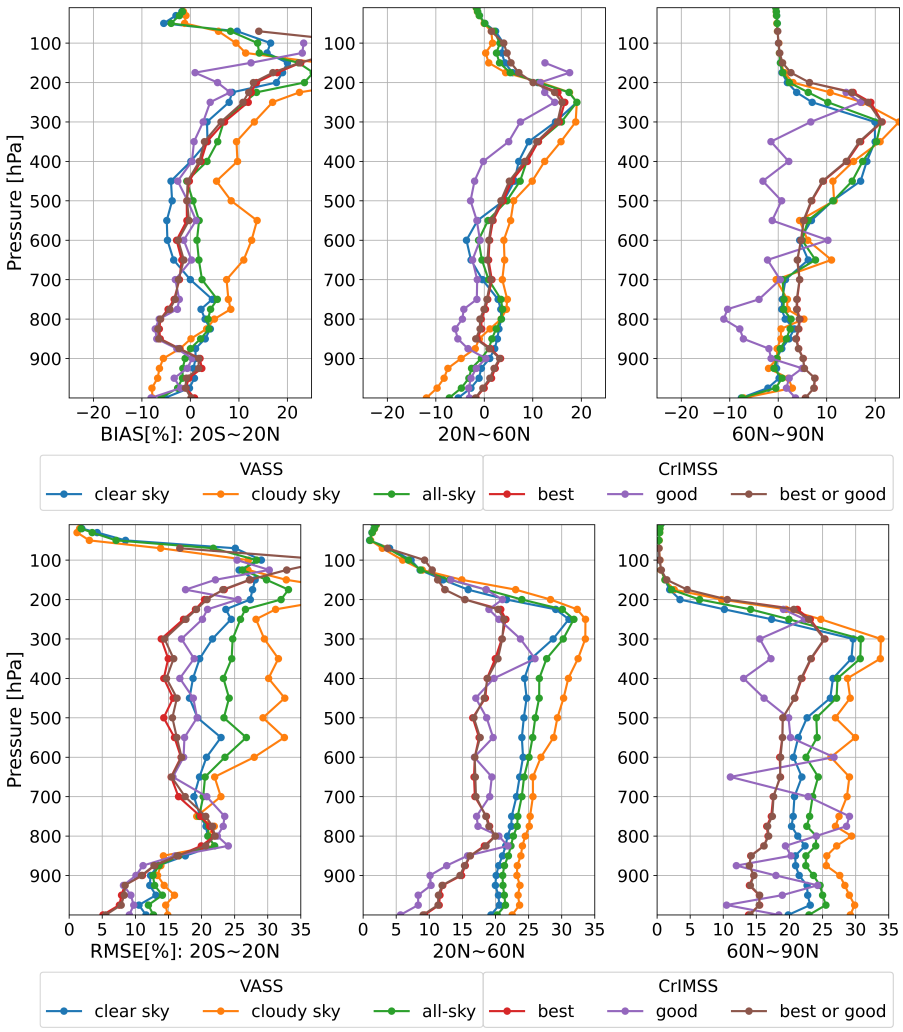

Fig. 8. Same as Fig. 7, but for humidity.

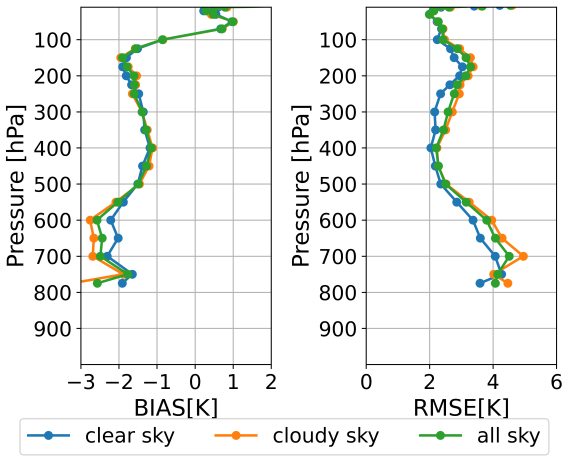

Fig. 9. Bias and RMSE of the VASS temperature profiles over the Tibetan Plateau.

comparison, CrIMSS biases are slightly higher, with best retrievals showing 5.82% overall and as high as 17.80% in the upper troposphere. The RMSE of VASS is generally higher than that of CrIMSS (best/good) at most levels, although VASS performs better between 250 hPa and 150 hPa. The mean RMSE values of VASS are 15.66% under clear sky (21.32%, 21.92%, and 24.27% for the lower, mid, and upper troposphere, respectively), 18.76% under cloudy sky (25.81%, 26.56%, and 27.21%), and 16.76% under all-sky conditions (22.85%, 23.52%, and 25.38%), while the RMSE values of CrIMSS range from 13.01% to 13.95% across quality flags. Despite higher RMSEs in the lower and middle troposphere, VASS represents the vertical structure of atmospheric humidity reasonably well.

Fig. 11 presents the comparison of temperature retrieval accuracy from VASS, GIIRS, and ERA5 against radiosonde observations over 134 common stations. ERA5 has the smallest bias overall, with values ranging between −1 K and 1 K across all pressure levels and a mean bias of −0.21 K. Its RMSE also remains consistently below 2 K, with a mean value of 1.54 K. This reflects the benefits of reanalysis data assimilation and long-term statistical optimization. VASS temperature retrievals under all-sky conditions show a mean bias of −0.80 K, with values ranging from −0.64 K (clear-sky) to −1.04 K (cloudy). Between 600 hPa and 250 hPa, the VASS bias under clear-

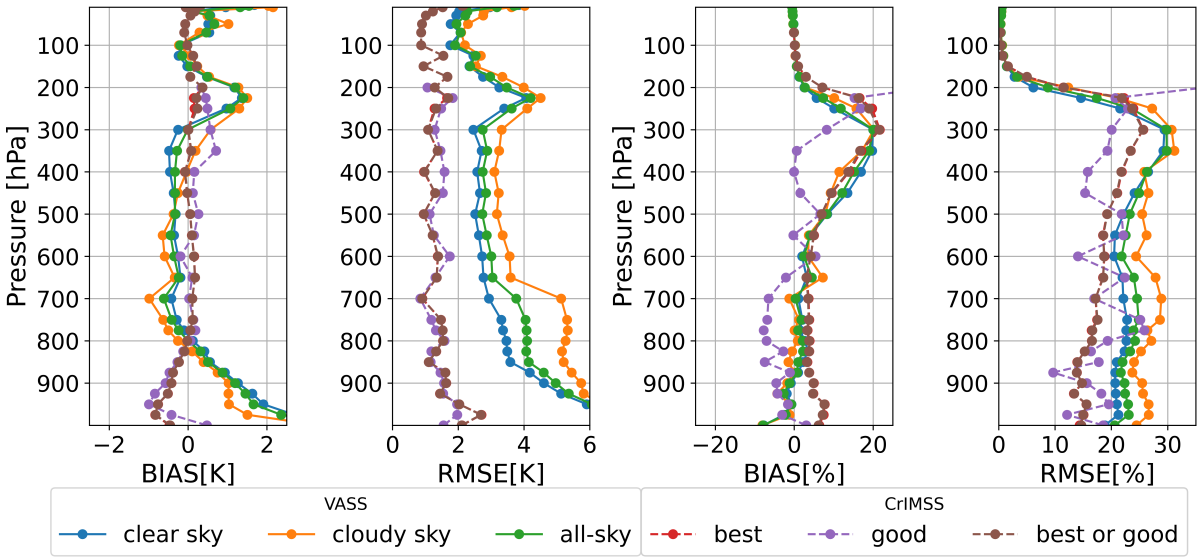

Fig. 10. Bias and RMSE for the VASS and CrIMSS temperature profiles. The legend is the same as that in Fig. 7.

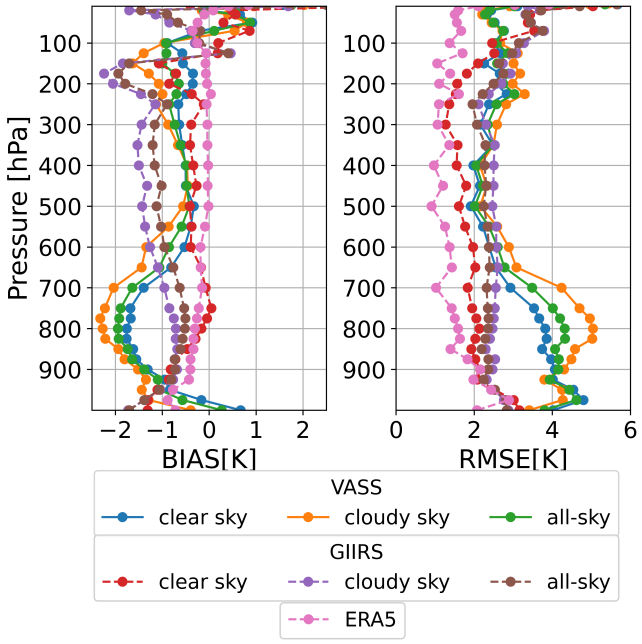

Fig. 11. Bias and RMSE of temperature profiles from VASS, GIIRS, and ERA5 compared to coincident radiosonde observations. The solid blue, orange, and green lines represent VASS retrievals under clear, cloudy, and all-sky conditions, respectively. The red, purple, and brown dashed lines indicate GIIRS retrievals under the same conditions, whereas the pink dashed line denotes ERA5.

sky conditions stays well within ±1 K, demonstrating stable retrieval performance in the mid-troposphere. Slightly larger biases are found in the lower troposphere (900–700 hPa), which is likely due to surface heterogeneity and increased cloud impact. This remains a challenge for infrared sounders in general. The mean RMSE of VASS temperature is 2.99 K, 3.34 K, and 3.14 K under clear, cloudy, and all-sky conditions, respectively. Although the RMSE of VASS is slightly higher than that of GIIRS below 650 hPa, the differences become marginal at higher altitudes. GIIRS retrievals show slightly lower bias in the lower troposphere, with mean biases of −0.22 K (clear), −1.03 K (cloudy), and −0.82 K (all-sky). The corresponding RMSE values are 2.28 K, 2.72 K, and 2.64 K. VASS performs comparably to GIIRS in capturing the thermal structure under clear-sky conditions, albeit with slightly larger uncertainties in the presence of clouds.

V. Conclusions

Accurate temperature and humidity profiles are essential for numerical weather prediction and climate monitoring. This study presents a comprehensive evaluation of FY-3E VASS temperature and humidity profiles from April 2023 to August 2024 using collocated radiosonde observations, satellite products (JPSS-1/CrIMSS, FY-4B/GIIRS) and ERA5 reanalysis data.

The VASS temperature retrievals show high consistency with radiosonde observations, achieving correlation coefficients above 0.99, which are comparable to those of the CrIMSS products. The correlation between the VASS humidity and radiosonde measurements is slightly lower than that of CrIMSS, but remains close to 0.80. The mean bias (RMSE) of VASS temperature retrievals is 0.63 K (3.07 K) under clear-sky conditions, 0.82 K (3.56 K) under cloudy skies, and 0.67 K (3.26 K) under all-sky conditions. For humidity, the mean bias (RMSE) is 4.63% (18.36%), 6.21% (21.38%), and 4.76% (19.36%) under clear, cloudy, and all-sky conditions, respectively. Overall, the retrievals meet the mission design requirements, although temperature errors remain larger than those from CrIMSS in the lower troposphere. When evaluated against coincident radiosonde data, the RMSE of VASS temperature is higher than that of CrIMSS, whereas the biases are close above 800 hPa. In terms of humidity, the VASS profiles show similar accuracy to CrIMSS, especially in the mid- and upper troposphere.

Compared with other infrared/microwave satellite products such as Aqua/AIRS (temperature accuracy: 1 K, humidity accuracy: 15%) [36], Aqua-AIRS/AMSU-A (1.0–2.5 K and 20–60%) [43], Aqua-AIRS/AMUS/HSB (1 K and 10%) [44], and Suomi-NPP CrIS/ATMS (0.82–1.16 K and 0.02–1.23 g kg^{-1}) [45], the accuracy of VASS retrievals satisfies the predesigned requirements for satellite-based temperature and humidity sounding. Although AIRS and CrIS have benefited from longer operational heritage, the FY-3E VASS retrievals already provide comparable accuracy and continue to improve with ongoing algorithm refinements.

The observed retrieval uncertainties can be attributed to several factors.

- Retrieval methodology: CrIMSS uses a classical OE approach, whereas VASS is based on a neural network framework. The VASS model was trained using ERA5 reanalysis data paired with co-located HIRAS and MWHS/MWTS observations during 2021–2022. Consequently, the retrieval performance for periods beyond the training window may be limited by the representativeness of the training dataset in terms of atmospheric variability.
- Bias in training data: ERA5 reanalysis is known to exhibit a cold bias of 0.2 to 1.5 K below 550 hPa compared to radiosonde observations [46], which can be inherited by the VASS temperature products. This helps explain the persistent cold bias observed in the mid- to lower troposphere.
- Cloud-related complexity: The higher RMSE in humidity under cloudy conditions reflects the increased complexity of cloud-radiation interactions and challenges of representing these effects in training data.
- Evaluation data coverage: The radiosonde network is unevenly distributed, with sparse coverage over oceans and polar regions, potentially biasing the validation results toward mid-latitude land areas.

The current version of the VASS algorithm is undergoing continuous refinement [16]. Future improvements will focus on expanding the training dataset, optimizing the neural network architecture, and enhancing cloud treatments. Improved representation of high-latitude and near-surface conditions will be especially valuable for data assimilation. Nevertheless, the FY-3E VASS products show strong potential for operational meteorological applications and data assimilation in numerical weather prediction models, particularly over observation-sparse regions like the polar areas and complex terrains. The capacity to provide consistent, near-real-time atmospheric profiles will continue to support global satellite sounding networks and contribute to both short-term weather forecasting and long-term climate monitoring.

Acknowledgments

The authors thank NSMC for providing the FY-3E VASS and FY-4B GIIRS data via the Fengyun Satellite Remote Sensing Data Service Network (https://satellite.nsmc.org.cn/). We also acknowledge NASA EOSDIS for access to JPSS-1 CrIMSS data through EARTHDATA (https://search.earthdata.nasa.gov/), and NOAA's NCEI for IGRA radiosonde data. The ERA5 reanalysis data were obtained from the Copernicus Climate Data Store. The authors are grateful to Dr. Yapeng Wang and Dr. Wenguang Bai from NSMC for their valuable guidance on the use of FY satellite data and retrieval algorithms.

References

[1] W. Wang, J. Xu, H. Letu, L. Zhang, Z. Wang, and J. Shi, "A new deep-learning-based framework for ice water path retrieval from microwave humidity sounder-ii aboard fengyun-3d satellite," *IEEE Transactions on Geoscience and Remote Sensing*, vol. 62, pp. 1–14, 2024.

[2] A. B. Milstein and W. J. Blackwell, "Neural network temperature and moisture retrieval algorithm validation for airs/amsu and cris/atms," *JOURNAL OF GEOPHYSICAL RESEARCH-ATMOSPHERES*, vol. 121, no. 4, pp. 1414–1430, FEB 27 2016.

[3] G. Tana, W. Lesi, H. Shang, J. Xu, D. Ji, J. Shi, H. Letu, and C. Shi, "A new cloud water path retrieval method based on geostationary satellite infrared measurements," *IEEE Transactions on Geoscience and Remote Sensing*, vol. 63, pp. 1–10, 2025.

[4] R. Monarrez, C. Barnet, N. Smith, A. Chang, E. Manning, P. Springer, and L. Iredell, "Nasa s-npp and noaa-20 (jpss-1) climcaps cris and atms level-2 products user guide: File format and definition," 2020.

[5] P. Rosenkranz, "Retrieval of temperature and moisture profiles from amsu-a and amsu-b measurements," *IEEE TRANSACTIONS ON GEOSCIENCE AND REMOTE SENSING*, vol. 39, no. 11, pp. 2429–2435, NOV 2001, international Geoscience and Remote Sensing Symposium (IGARSS 00), HONOLULU, HI, JUL 24-28, 2000.

[6] A. Doherty, N. Atkinson, W. Bell, and A. Smith, "An assessment of data from the advanced technology microwave sounder at the met office," *ADVANCES IN METEOROLOGY*, vol. 2015, 2015.

[7] N. Livesey, W. Van Snyder, W. Read, and P. Wagner, "Retrieval algorithms for the eos microwave limb sounder (mls)," *IEEE Transactions on Geoscience and Remote Sensing*, vol. 44, no. 5, pp. 1144–1155, 2006.

[8] J. Susskind, C. Barnet, and J. Blaisdell, "Retrieval of atmospheric and surface parameters from airs/amsu/hsb data in the presence of clouds," *IEEE Transactions on Geoscience and Remote Sensing*, vol. 41, no. 2, pp. 390–409, 2003.

[9] M. W. Shephard, S. A. Clough, V. H. Payne, W. L. Smith, S. Kireev, and K. E. Cady-Pereira, "Performance of the line-by-line radiative transfer model (lblrtm) for temperature and species retrievals: Iasi case studies from jaivex," *ATMOSPHERIC CHEMISTRY AND PHYSICS*, vol. 9, no. 19, pp. 7397–7417, 2009.

[10] C. D. Barnet, N. Smith, K. Ide, K. Garrett, and E. Jones, "Evaluating the value of cris shortwave-infrared channels in atmospheric-sounding retrievals," *REMOTE SENSING*, vol. 15, no. 3, FEB 2023.

[11] P. Rosenkranz, "Rapid radiative transfer model for amsu/hsb channels," *IEEE TRANSACTIONS ON GEOSCIENCE AND REMOTE SENSING*, vol. 41, no. 2, pp. 362–368, FEB 2003.

[12] R. Bonsignori, "The microwave humidity sounder (mhs): In-orbit performance assessment," *Proc. SPIE 6744, Sensors, Systems, and Next-Generation Satellites XI*, vol. 67440A, 10 2007.

[13] I. Moradi, R. R. Ferraro, B. J. Soden, P. Eriksson, and P. Arkin, "Retrieving layer-averaged tropospheric humidity from advanced technology microwave sounder water vapor channels," *IEEE TRANSACTIONS ON GEOSCIENCE AND REMOTE SENSING*, vol. 53, no. 12, pp. 6675–6688, DEC 2015.

[14] M. L. Feltz, L. Borg, R. O. Knuteson, D. Tobin, H. Revercomb, and A. Gambacorta, "Assessment of noaa nucaps upper air temperature profiles using cosmic gps radio occultation and arm radiosondes," *Journal of Geophysical Research: Atmospheres*, vol. 122, no. 17, pp. 9130–9153, 2017. [Online]. Available: https://agupubs.onlinelibrary.wiley.com/doi/abs/10.1002/2017JD026504

[15] N. Smith and C. D. Barnet, "Climcaps—a nasa long-term product for infrared + microwave atmospheric soundings," *Earth and Space Science*, vol. 10, no. 5, p. e2022EA002701, 2023, e2022EA002701 2022EA002701. [Online]. Available: https://agupubs.onlinelibrary.wiley.com/doi/abs/10.1029/2022EA002701

[16] W. Bai, P. Zhang, H. Liu, W. Zhang, C. Qi, G. Ma, and G. Li, "A fast piecewise-defined neural network method to retrieve temperature and humidity profile for the vertical atmospheric sounding system of fengyun-3e satellite," *IEEE TRANSACTIONS ON GEOSCIENCE AND REMOTE SENSING*, vol. 61, 2023.

[17] P. Zhang, X. Hu, Q. Lu, A. Zhu, M. Lin, L. Sun, L. Chen, and N. Xu, "Fy-3e: The first operational meteorological satellite mission in an early morning orbit," *ADVANCES IN ATMOSPHERIC SCIENCES*, vol. 39, no. 1, pp. 1–8, 2022.

[18] J. M. Wallace and P. V. Hobbs, *Atmospheric Science: An Introductory Survey*, 2nd ed. San Diego: Academic Press, 2006. [Online]. Available: https://www.elsevier.com/books/atmospheric-science/wallace/978-0-12-732951-2

[19] N. Smith and C. D. Barnet, "Uncertainty characterization and propagation in the community long-term infrared microwave combined atmospheric product system (climcaps)," *REMOTE SENSING*, vol. 11, no. 10, MAY 2 2019.

[20] C. Barnet, "Sounder sips: Suomi npp crimss level 2 climcaps normal spectral resolution: Atmosphere cloud and surface geophysical state v2, greenbelt, md, usa, goddard earth sciences data and information services center (ges disc), accessed: [october 23, 2024]," 2019.

[21] ——, "Sounder sips: Jpss-1 cris level 2 climcaps: Atmosphere cloud and surface geophysical state v2, greenbelt, md, usa, goddard earth sciences data and information services center (ges disc), accessed: [20241105]," 2024.

[22] H. T. Thrastarson, E. J. Fetzer, S. Ray, T. Hearty, and N. Smith, *Overview of the AIRS mission: Instruments, processing algorithms, products, and documentation (edition 2.0; the AIRS-team and the CLIMCAPS algorithms)*, Jet Propulsion Laboratory, 2021, available at https://docserver.gesdisc.eosdis.nasa.gov/public/project/AIRS/Overview_of_the_AIRS_Mission.pdf.

[23] National Satellite Meteorological Center (NSMC). (2025) Giirs instrument. [Online]. Available: https://www.nsmc.org.cn/nsmc/cn/instrument/GIIRS.html [Accessed: 2025-05-15]. [Online]. Available: https://www.nsmc.org.cn/nsmc/cn/instrument/GIIRS.html

[24] H. Liu, W. Bai, G. Ma, G. Wang, P. Zhang, W. Zhang, J. Li, X. Wang, Q. Shen, and Y. Ao, "Neural network temperature and moisture retrieval technique for real-time processing of fengyun-4b/giirs hyperspectral radiances," *METEOROLOGY AND ATMOSPHERIC PHYSICS*, vol. 136, no. 5, OCT 2024.

[25] I. Durre, X. Yin, R. S. Vose, S. Applequist, and J. Arnfield, "Enhancing the data coverage in the integrated global radiosonde archive," *Journal of Atmospheric and Oceanic Technology*, vol. 35, no. 9, pp. 1753 – 1770, 2018. [Online]. Available: https://journals.ametsoc.org/view/journals/atot/35/9/jtech-d-17-0223.1.xml

[26] S. Li, T. Xu, N. Jiang, Y. Xu, H. Yang, and L. Bastos, "Assessment of the atmosphere profiles and derived parameters from fresh fengyun-3e and other common occultation systems," *MEASUREMENT*, vol. 228, MAR 31 2024.

[27] G. S. Gopikrishnan, J. Kuttippurath, and P. K. Thapliyal, "Assessment of relative humidity measurements from insat-3d/3dr sounder with radiosonde and satellite measurements over india," *JOURNAL OF THE INDIAN SOCIETY OF REMOTE SENSING*, 2024 SEP 25 2024.

[28] G. S. Gopikrishnan, J. Kuttippurath, P. K. Thapliyal, and M. V. Shukla, "Validation of insat-3d and insat-3dr temperature profile retrievals using ground-based, satellite, and reanalysis data," *JOURNAL OF GEOPHYSICAL RESEARCH-ATMOSPHERES*, vol. 128, no. 22, NOV 27 2023.

[29] Y. Li, Y. Yuan, and X. Wang, "Assessments of the retrieval of atmospheric profiles from gnss radio occultation data in moist tropospheric conditions using radiosonde data," *REMOTE SENSING*, vol. 12, no. 17, SEP 2020.

[30] F. Di Paola, E. Ricciardelli, D. Cimini, A. Cersosimo, A. Di Paola, D. Gallucci, S. Gentile, E. Geraldi, S. Larosa, S. T. Nilo, E. Ripepi, F. Romano, P. Sano, and M. Viggiano, "Mirtaw: An algorithm for atmospheric temperature and water vapor profile estimation from atms measurements using a random forests technique," *REMOTE SENSING*, vol. 10, no. 9, SEP 2018.

[31] M. He, D. Wang, W. Ding, Y. Wan, Y. Chen, and Y. Zhang, "A validation of fengyun4a temperature and humidity profile products by radiosonde observations," *Remote Sensing*, vol. 11, no. 17, 2019.

[32] F. Iturbide-Sanchez, S. R. S. da Silva, Q. Liu, K. L. Pryor, M. E. Pettey, and N. R. Nalli, "Toward the operational weather forecasting application of atmospheric stability products derived from nucaps cris/atms soundings," *IEEE TRANSACTIONS ON GEOSCIENCE AND REMOTE SENSING*, vol. 56, no. 8, pp. 4522–4545, AUG 2018.

[33] M. D. Goldberg, H. Kilcoyne, H. Cikanek, and A. Mehta, "Joint polar satellite system: The united states next generation civilian polar-orbiting environmental satellite system," *JOURNAL OF GEOPHYSICAL RESEARCH-ATMOSPHERES*, vol. 118, no. 24, pp. 13 463–13 475, DEC 27 2013.

[34] N. Smith and C. D. Barnet, "Climcaps observing capability for temperature, moisture, and trace gases from airs/amsu and cris/atms," *ATMOSPHERIC MEASUREMENT TECHNIQUES*, vol. 13, no. 8, pp. 4437–4459, AUG 17 2020.

[35] I. Durre, R. Vose, and D. Wuertz, "Overview of the integrated global radiosonde archive," *JOURNAL OF CLIMATE*, vol. 19, no. 1, pp. 53–68, JAN 1 2006.

[36] M. Divakarla, C. Barnet, M. Goldberg, L. McMillin, E. Maddy, W. Wolf, L. Zhou, and X. Liu, "Validation of atmospheric infrared sounder temperature and water vapor retrievals with matched radiosonde measurements and forecasts," *JOURNAL OF GEOPHYSICAL RESEARCH ATMOSPHERES*, vol. 111, no. D9, APR 6 2006.

[37] L. Zhang, S. Tie, Q. He, and W. Wang, "Performance analysis of the temperature and humidity profiles retrieval for fy-3d/mwths in arctic regions," *REMOTE SENSING*, vol. 14, no. 22, NOV 2022.

[38] R. Fan, L. Zhang, J. Chen, T. Wei, W. Huang, B. Tian, and M. Ding, "Comprehensive assessment of airs, tshs, and vass temperature profile products in the arctic land region," *ADVANCES IN ATMOSPHERIC SCIENCES*, vol. 42, no. 7, pp. 1499–1512, JUL 2025.

[39] B. Sun, A. Reale, D. J. Seidel, and D. C. Hunt, "Comparing radiosonde and cosmic atmospheric profile data to quantify differences among radiosonde types and the effects of imperfect collocation on comparison statistics," *JOURNAL OF GEOPHYSICAL RESEARCH-ATMOSPHERES*, vol. 115, DEC 3 2010.

[40] X. Meng, H. Guo, J. Cheng, and B. Yao, "Can the era5 reanalysis product improve the atmospheric correction accuracy of landsat series thermal infrared data?" *IEEE GEOSCIENCE AND REMOTE SENSING LETTERS*, vol. 19, 2022.

[41] Y. Zhang, B. Lin, and D. Zheng, "A discussion on the boundary and area of the tibetan plateau in china," *GEOGRAPHICAL RESEARCH*, vol. 21, no. 1, pp. 1–8, JAN 2002.

[42] P. Shi, Y. Chen, G. Zhang, H. Tang, Z. Chen, D. Yu, J. Yang, T. Ye, J. Wang, S. Liang, Y. Ma, J. Wu, and P. Gong, "Factors contributing to spatial-temporal variations of observed oxygen concentration over the qinghai-tibetan plateau," *SCIENTIFIC REPORTS*, vol. 11, no. 1, AUG 30 2021.

[43] M. Diao, L. Jumbam, J. Sheffield, E. F. Wood, and M. A. Zondlo, "Validation of airs/amsu-a water vapor and temperature data with in situ aircraft observations from the surface to ut/ls from 87°n-67°s," *JOURNAL OF GEOPHYSICAL RESEARCH-ATMOSPHERES*, vol. 118, no. 12, pp. 6816–6836, JUN 27 2013.

[44] E. Fetzer, L. McMillin, D. Tobin, H. Aumann, M. Gunson, W. McMillan, D. Hagan, M. Hofstadter, J. Yoe, D. Whiteman, J. Barnes, R. Bennartz, H. Vömel, V. Walden, M. Newchurch, P. Minnett, R. Atlas, F. Schmidlin, E. Olsen, M. Goldberg, S. Zhou, H. Ding, W. Smith, and H. Revercomb, "Airs/amsu/hsb validation," *IEEE TRANSACTIONS ON GEOSCIENCE AND REMOTE SENSING*, vol. 41, no. 2, pp. 418–431, FEB 2003.

[45] N. R. Nalli, A. Gambacorta, Q. Liu, C. D. Barnet, C. Tan, F. Iturbide-Sanchez, T. Reale, B. Sun, M. Wilson, L. Borg, and V. R. Morris, "Validation of atmospheric profile retrievals from the snpp noaa-unique combined atmospheric processing system. part 1: Temperature and moisture," *IEEE Transactions on Geoscience and Remote Sensing*, vol. 56, no. 1, pp. 180–190, 2018.

[46] M. Virman, M. Bister, J. Raisanen, V. A. Sinclair, and H. Jarvinen, "Radiosonde comparison of era5 and era-interim reanalysis datasets over tropical oceans," *TELLUS SERIES A-DYNAMIC METEOROLOGY AND OCEANOGRAPHY*, vol. 73, no. 1, JAN 1 2021.